Model Predictive Control of a Multilevel Current Source Inverter Together with its Current Source

Pablo Cossutta
Mathias Angelico Engelhardt
Miguel Aguirre
CIDEI - ITBA
Instituto Tecnológico de Buenos Aires
Buenos Aires, Argentina
pcossutt@itba.edu.ar

Juan Ponce
CONICET - CIDEI - ITBA
Consejo Nacional de Investigaciones Científicas y Técnicas
Instituto Tecnológico de Buenos Aires
Buenos Aires, Argentina
jponce@itba.edu.ar

María Inés Valla
LEICI - UNLP
Laboratorio de Electrónica Industrial, Control e Instrumentación
Universidad Nacional de La Plata
La Plata, Argentina
m.i.valla@ieee.org

***Abstract*—In this paper, a Model Predictive Control (MPC) strategy is applied to a Multilevel Current Source Inverter (MCSI) and its associated current source. The controller uses a discrete-time model of the entire system in order to predict the future behavior for each of the available switch states. The system is composed of a multilevel inverter, a buck converter, an output filter and a load. Each of the calculated values is used to minimize a set of predefined control objectives within a multi-term cost function. It includes costs associated with the switching frequency and reference tracking. This allows to control not only the output voltages of the load, but also the current source and the balance of the internal currents of the inverter. Simulation results show a good performance and fast dynamics with a low switching frequency of all the switches involved. These features make the proposed controller a suitable option for use with high power converters.**

***Index Terms*—Model Predictive Control, Multilevel Current Source Inverter, Current Source Inverter.**

I. Introduction

The need for efficient energy generation and storage from renewable energy sources is attracting a great amount of resources worldwide [1], [2]. Research related to multilevel converters has increased in recent years due to many factors, like reducing the harmonic distortion introduced at the load, using lower voltage or current semiconductors and reducing the size of internal storage components (capacitors and inductors) with lower voltage and current rates. Both, the Current Source Inverter (CSI) and the Multilevel Current Source Inverter (MCSI) can be used with different energy sources as an interface between them and the utility grid [3]. Multilevel topologies can be used to connect various forms of energy to the power grid at the expense of increasing its complexity and a higher control effort. The MCSI is a good choice because of its high reliability, fault tolerant operation, quasi soft switching and the use of capacitors of low value among others. Traditionally, the MCSI is controlled using linear control loops, usually a Proportional Integral controller (PI), a rotating frame coordinate transformation and a modulation stage [4]–[7]. A new kind of controllers based on the Finite Control Set of Model Predictive Control (FCS-MPC) strategy can be found in the literature [8]–[10]. They have been used in several types of voltage converters showing a robust response under different load conditions. They alsa have been used with different control objectives, such as improving the dynamics of a converter, balancing the internal currents and reducing the switching frequency among others [11]–[14].

The operation of the FCS-MPC controller is based on using the discrete-time mathematical model of the converter to predict the future behavior. In general, the prediction horizon can be increased to achieve a better performance. However in this paper, a prediction horizon of one sample is used to achieve good resolution with low computing requirements. The predicted values of interest are used to evaluate a cost function in order to achieve a good reference tracking, operate at a low switching frequency and reduce the Total Harmonic Distortion (THD) of the output waveforms. The controller will select and apply the switching state that minimizes the cost function and meets the control objectives.

The MCSI topology is fed by a current source which can be implemented using a buck converter driven by a voltage source. This topology is suitable for building a constant current source from renewable energy sources such as fuel cells [15], [16], solar panels [17], [18] or wind generators among others. The buck converter allows to control the energy delivered to the MCSI even when the voltage source varies its value within a given range.

In this paper, the predictive control strategy of the MCSI along with the buck converter is presented. Mathematical models of both converters are used to control the output voltage and input current of the MCSI, while achieving low switching frequencies and low THD of the output waveforms.

II. Overall System Model

A. Topology

The entire system is shown in Fig. 1. It is composed of a voltage source, a current buck converter and a MCSI converter. The MCSI is composed of three identical modules connected in parallel and in series with two main inductors L_{dc}. Each of the modules is a conventional CSI in series with two sharing inductors L. They consist of six reverse blocking switches that could be implemented with either insulated gate bipolar

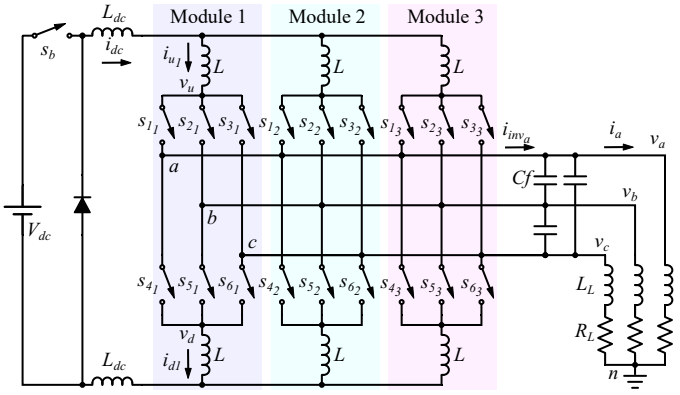

Fig. 1. Topology

transistors (IGBT) each one with a series diode to block the reverse current or integrated gate commutated thyristors (IGCT) among others. A three phase capacitor is placed at the output to improve the Total Harmonic Distortion (THD) in both, current and voltage waveforms of the load. The input current of the MCSI i_{dc} is delivered by the buck converter.

B. Mathematical Model of the System

The predictive control strategy requires the mathematical model of the entire system to predict the values of interest for each one of the valid switch states. At any instant of time, each module of the multilevel converter must guarantee a valid path for the current, therefore only one of the upper switches and one of the lower switches must be closed. Thus, the deterministic behavior of the system is guaranteed and the output current is well defined, only depending on the condition of the switches and the current source. This restriction is stated as

$$s_{1_x} + s_{2_x} + s_{3_x} = s_{4_x} + s_{5_x} + s_{6_x} = 1 \quad x \in \{1,2,3\} \quad (1)$$

where x is the module number. Table I shows each of the nine possible switches state for each module. Where i_{a_x}, i_{b_x} and i_{c_x} are the output currents of each module and v_{ud} is the equivalent voltage between the terminals u and d of the module x. Since there are three modules, each one with 9 different switching states, there are $9^3 = 729$ possible combinations that provide 7 different levels of current at the output. The system modeling is performed by splitting it into two interconnected subsystems: one involves the converter with its current source and the other is composed of the filter capacitors and load. Applying the laws of Kirchoff, the 7 equations that define the first subsystem are obtained

$$\begin{cases} i_{dc} &= i_{u_1} + i_{u_2} + i_{u_3} \\ i_{dc} &= i_{d_1} + i_{d_2} + i_{d_3} \\ V_{dc}\, s_b &= 2\, L_{dc}\, \dot{i}_{dc} + L\, \dot{i}_{u_1} + v_{un_1} + v_{nd_1} + L\, \dot{i}_{d_1} \\ V_{dc}\, s_b &= 2\, L_{dc}\, \dot{i}_{dc} + L\, \dot{i}_{u_2} + v_{un_2} + v_{nd_2} + L\, \dot{i}_{d_2} \\ V_{dc}\, s_b &= 2\, L_{dc}\, \dot{i}_{dc} + L\, \dot{i}_{u_3} + v_{un_3} + v_{nd_3} + L\, \dot{i}_{d_3} \\ V_{dc}\, s_b &= 2\, L_{dc}\, \dot{i}_{dc} + L\, \dot{i}_{u_1} + v_{un_1} + v_{nd_2} + L\, \dot{i}_{d_2} \\ V_{dc}\, s_b &= 2\, L_{dc}\, \dot{i}_{dc} + L\, \dot{i}_{u_2} + v_{un_2} + v_{nd_3} + L\, \dot{i}_{d_3} \end{cases} \quad (2)$$

TABLE I
OUTPUT CURRENT AND VOLTAGE v_{ud} OF MODULE x

State	s_{1_x}	s_{2_x}	s_{3_x}	s_{4_x}	s_{5_x}	s_{6_x}	i_{a_x}	i_{b_x}	i_{c_x}	v_{ud_x}
#1	1	0	0	1	0	0	i_{u_x}-i_{d_x}	0	0	0
#2	1	0	0	0	1	0	i_{u_x}	-i_{d_x}	0	v_{ab}
#3	1	0	0	0	0	1	i_{u_x}	0	-i_{d_x}	v_{ac}
#4	0	1	0	1	0	0	-i_{d_x}	i_{u_x}	0	v_{ba}
#5	0	1	0	0	1	0	0	i_{u_x}-i_{d_x}	0	0
#6	0	1	0	0	0	1	0	i_{u_x}	-i_{d_x}	v_{bc}
#7	0	0	1	1	0	0	-i_{d_x}	0	i_{u_x}	v_{ca}
#8	0	0	1	0	1	0	0	-i_{d_x}	i_{u_x}	v_{cb}
#9	0	0	1	0	0	1	0	0	i_{u_x}-i_{d_x}	0

Where s_b is the state of the switch that controls the current source. As i_{dc} is linearly dependant, it can be eliminated from the state equations. Voltages v_{un_x} and v_{nd_x} are the voltages between node u and n and between n and d respectively. They are expressed as a function of the switches state in the form s_{1-6_x} where x represents the module.

$$\begin{bmatrix} v_{un_1} \\ v_{un_2} \\ v_{un_3} \end{bmatrix} = \begin{bmatrix} s_{1_1} & s_{2_1} & s_{3_1} \\ s_{1_2} & s_{2_2} & s_{3_2} \\ s_{1_3} & s_{2_3} & s_{3_3} \end{bmatrix} \begin{bmatrix} v_a \\ v_b \\ v_c \end{bmatrix}$$
$$\begin{bmatrix} v_{nd_1} \\ v_{nd_2} \\ v_{nd_3} \end{bmatrix} = - \begin{bmatrix} s_{4_1} & s_{5_1} & s_{6_1} \\ s_{4_2} & s_{5_2} & s_{6_2} \\ s_{4_3} & s_{5_3} & s_{6_3} \end{bmatrix} \begin{bmatrix} v_a \\ v_b \\ v_c \end{bmatrix} \quad (3)$$

The output current of the inverter i_{inv_x} is defined by the state of the switches s_{1-6_x} as follows

$$\begin{bmatrix} i_{inv_a} \\ i_{inv_b} \\ i_{inv_c} \end{bmatrix} = \begin{bmatrix} s_{1_1} & s_{1_2} & s_{1_3} \\ s_{2_1} & s_{2_2} & s_{2_3} \\ s_{3_1} & s_{3_2} & s_{3_3} \end{bmatrix} \begin{bmatrix} i_{u_1} \\ i_{u_2} \\ i_{u_3} \end{bmatrix} - \begin{bmatrix} s_{4_1} & s_{4_2} & s_{4_3} \\ s_{5_1} & s_{5_2} & s_{5_3} \\ s_{6_1} & s_{6_2} & s_{6_3} \end{bmatrix} \begin{bmatrix} i_{d_1} \\ i_{d_2} \\ i_{d_3} \end{bmatrix} \quad (4)$$

Finally, the state space representation of this subsystem is

$$\begin{bmatrix} \dot{i}_{u_1} \\ \dot{i}_{u_2} \\ \dot{i}_{u_3} \\ \dot{i}_{d_1} \\ \dot{i}_{d_2} \\ \dot{i}_{d_3} \end{bmatrix} = \frac{a}{3} \begin{bmatrix} b & c & c & 1 & 1 & 1 \\ c & b & c & 1 & 1 & 1 \\ c & c & b & 1 & 1 & 1 \\ 1 & 1 & 1 & b & c & c \\ 1 & 1 & 1 & c & b & c \\ 1 & 1 & 1 & c & c & b \end{bmatrix} \begin{bmatrix} v_{un_1} \\ v_{un_2} \\ v_{un_3} \\ v_{nd_1} \\ v_{nd_2} \\ v_{nd_3} \end{bmatrix} + a\, s_b \begin{bmatrix} 1 \\ 1 \\ 1 \\ 1 \\ 1 \\ 1 \end{bmatrix} V_{dc} \quad (5)$$

$$a = \frac{1}{2\,(L + 3\,L_{dc})} \quad b = 5 + 12\frac{L}{L_{dc}} \quad c = -1 - 6\frac{L}{L_{dc}}$$

The second subsystem that models the load and the filter capacitors is defined by

$$\begin{cases} \dot{v_x} = \dfrac{i_{invx} - i_x}{3\,C_f} \\ \dot{i_x} = \dfrac{v_x - R_L\, i_x}{L_L} \end{cases} \quad x \in \{a,b,c\} \quad (6)$$

Where C_f is the filter capacitance, L_L the load inductance and R_L the load resistance. This subsystem inputs, i_{inv_x} are

outputs from the previous one. Expressing the above equations in a state space representation format,

$$\begin{bmatrix} \dot{v}_a \\ \dot{v}_b \\ \dot{v}_c \\ \dot{i}_a \\ \dot{i}_b \\ \dot{i}_c \end{bmatrix} = \begin{bmatrix} 0 & 0 & 0 & d & 0 & 0 \\ 0 & 0 & 0 & 0 & d & 0 \\ 0 & 0 & 0 & 0 & 0 & d \\ e & 0 & 0 & f & 0 & 0 \\ 0 & e & 0 & 0 & f & 0 \\ 0 & 0 & e & 0 & 0 & f \end{bmatrix} \begin{bmatrix} v_a \\ v_b \\ v_c \\ i_a \\ i_b \\ i_c \end{bmatrix} - d \begin{bmatrix} i_{inv_a} \\ i_{inv_b} \\ i_{inv_c} \\ 0 \\ 0 \\ 0 \end{bmatrix} \tag{7}$$

$$d = -\frac{1}{3\,C_f} \qquad e = \frac{1}{L_L} \qquad f = -eR_L$$

III. Model Predictive Control Strategy

The equations of the previous section define the dynamic behavior of the system. The predictive control strategies currently found in the literature are based on the use of a discrete-time model of the plant. By using the mathematical model, the prediction of the state variables of the system for each possible switching state is obtained. The controller uses these results to obtain the control action that best meets the objectives defined in a global cost function.

A. Prediction Model

Since the previous equations are in continuous-time, it is necessary to obtain its discrete representation so the forward Euler transformation is used. According to this transformation, the derivative of a generic variable x can be approximated as

$$\dot{x} = \frac{x_{k+1} - x_k}{T_s} \tag{8}$$

where T_s is the sampling time. Applying (8) in (5),

$$\begin{bmatrix} i_{u_1} \\ i_{u_2} \\ i_{u_3} \\ i_{d_1} \\ i_{d_2} \\ i_{d_3} \end{bmatrix}_{k+1} = \frac{aT_s}{3} \begin{bmatrix} b & c & c & 1 & 1 & 1 \\ c & b & c & 1 & 1 & 1 \\ c & c & b & 1 & 1 & 1 \\ 1 & 1 & 1 & b & c & c \\ 1 & 1 & 1 & c & b & c \\ 1 & 1 & 1 & c & c & b \end{bmatrix} \begin{bmatrix} v_{un_1} \\ v_{un_2} \\ v_{un_3} \\ v_{nd_1} \\ v_{nd_2} \\ v_{nd_3} \end{bmatrix}_k + \begin{bmatrix} i_{u_1} \\ i_{u_2} \\ i_{u_3} \\ i_{d_1} \\ i_{d_2} \\ i_{d_3} \end{bmatrix}_k + aT_s s_b \begin{bmatrix} 1 \\ 1 \\ 1 \\ 1 \\ 1 \\ 1 \end{bmatrix} V_{dc} \tag{9}$$

In a similar way, using (8) and (7), the discrete time representation of the other subsystem is obtained.

$$\begin{bmatrix} v_a \\ v_b \\ v_c \\ i_a \\ i_b \\ i_c \end{bmatrix}_{k+1} = \begin{bmatrix} 1 & 0 & 0 & d' & 0 & 0 \\ 0 & 1 & 0 & 0 & d' & 0 \\ 0 & 0 & 1 & 0 & 0 & d' \\ e' & 0 & 0 & f' & 0 & 0 \\ 0 & e' & 0 & 0 & f' & 0 \\ 0 & 0 & e' & 0 & 0 & f' \end{bmatrix} \begin{bmatrix} v_a \\ v_b \\ v_c \\ i_a \\ i_b \\ i_c \end{bmatrix}_k - d' \begin{bmatrix} i_{inv_a} \\ i_{inv_b} \\ i_{inv_c} \\ 0 \\ 0 \\ 0 \end{bmatrix}_k \tag{10}$$

$$d' = -\frac{T_s}{3\,C_f} \qquad e' = \frac{T_s}{L_L} \qquad f' = 1 - e'\,R_L$$

As detailed in (10), the voltages and currents at the load change one sampling time after the output currents of the inverter change, which is achieved by a change in the switch states $s_{1-6_{1-3}}$ at time k. Besides, (9) shows that the internal currents of the converter vary a sampling time after the switch s_b is modified. The controller must take into account 1458 possible combinations of switching states at each sampling time, since there are 729 different switch states for the modules and 2 possible switch states for the current source. In addition, the controller must calculate the prediction of the state variables and compute which one of these predictions minimizes the global cost function. This is a time consuming task and requires a high computing power. Therefore, to take into account the delay introduced by the computation, the predictive controller outputs at time k will be applied at the time instant $k+1$. This imposes the restriction that all the calculations necessary to perform the predictive control must be performed in less than T_s seconds.

Therefore, at every sampling instant k, a new set of measurements of the system v_{a,b,c_k}, i_{a,b,c_k}, $i_{u1,2,3_k}$, $i_{d1,2,3_k}$ are obtained. Based on these measurements at time k and the optimal states calculated in the previous instant, predictions are calculated for time $k+1$ using (3), (4), (9) and (10). In these equations only the switching states generated in the sampling instant $k-1$ by the predictive controller are used.

With the predictions at time $k+1$ and using again (3), (4), (9) and (10), the predictions at instant $k+2$ are computed, modifying subscripts $k+1$ by $k+2$ and k by $k+1$ in those equations. Thus, the predictions at time $k+2$ are obtained for each of the valid combinations of the 19 switches of the system.

B. Cost Function Optimization

After obtaining the set of system state variables for each possible combination of switches at time $k+2$, the controller must select the one that best meets the control objectives. A global multi-term cost function is defined where each term is associated with a specific control objective. The combination that produces the lowest cost is selected by the controller.

The first term of the cost function, related to the output voltages at the load, is defined by the sum of the quadratic errors with respect to a voltage reference

$$\begin{aligned} c_{v_{ref}} = (v_{a_{k+2}} - v^*_{a_{k+2}})^2 + (v_{b_{k+2}} - v^*_{b_{k+2}})^2 \\ + (v_{c_{k+2}} - v^*_{c_{k+2}})^2 \end{aligned} \tag{11}$$

Given a current reference, $i_{dc_{ref}}$, taking into account (2)a-b and considering that currents $i_{u_{1,2,3}}$ and $i_{d_{1,2,3}}$ must be equal to each other, the internal currents must be equal to $\frac{i_{dc_{ref}}}{3}$. The cost term associated with the current reference results,

$$c_{i_{dc}} = \sum_{x=1}^{3} \left[\left(i_{u_{x_{k+2}}} - \frac{i_{dc_{ref}}}{3} \right)^2 + \left(i_{d_{x_{k+2}}} - \frac{i_{dc_{ref}}}{3} \right)^2 \right] \tag{12}$$

Since the voltage references are the inputs of the control system known at instant k and as the prediction is made for instant $k+2$, a prediction of the references is needed. In order to make the prediction, a fourth order Lagrange extrapolation is used, given by

$$v^*_{k+1} = 4v^*_k - 6v^*_{k-1} + 4v^*_{k-2} - v^*_{k-3} \tag{13}$$

By applying (13) again, the references at instant $k+2$ are

$$v^*_{k+2} = 10v^*_k - 20v^*_{k-1} + 15v^*_{k-2} - 4v^*_{k-3} \tag{14}$$

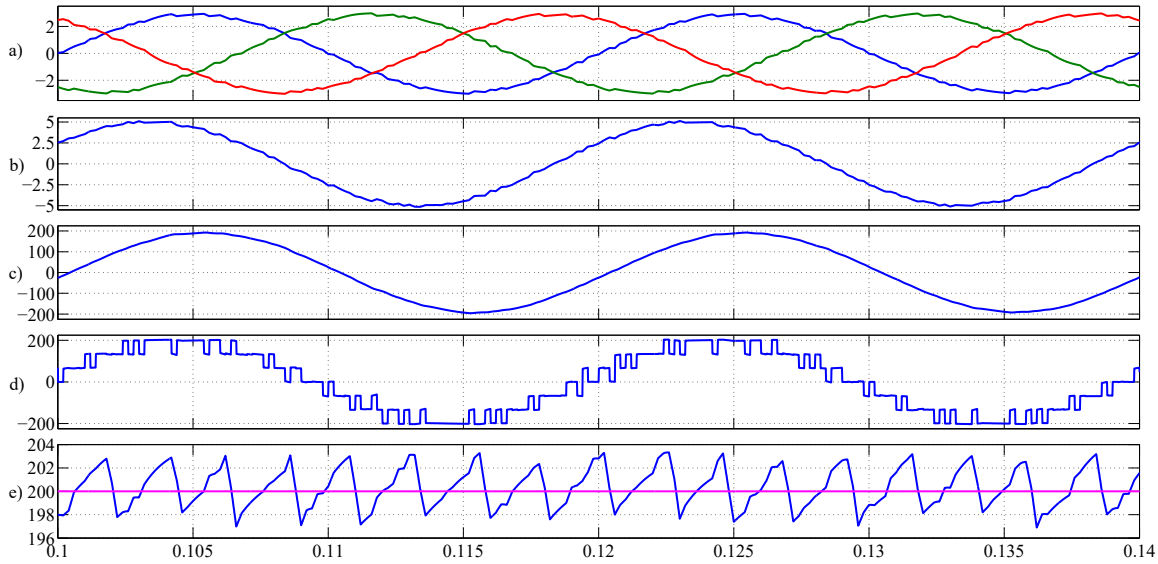

Fig. 2. Simulation results under nominal conditions; a) phase voltages and references [kV], b) line-to-line output voltage v_{ab} [kV], c) output current i_a [A], d) inverter output current of phase a [A], e) inductor current i_{dc} [A]

According to the literature, this estimation can be used for a wide range of frequencies of v^*. Since the sampling time is small enough and the signal is a sine wave at line frequency the extrapolation is valid and hence used.

This predictive control strategy allows the inclusion of other constraints within the global cost function. In this kind of systems, it is desirable to reduce the switching frequency and improve the efficiency, reducing power losses due to the commutation of the switches. A term that penalizes state transitions that produce the greatest number of changes in switching states from one sampling time to the next is added to the cost function. The number of switches that change at each sampling time is

$$N_{comm} = \sum_{x=1}^{3} \sum_{i=1}^{6} \left| s_{i_{x_{k+1}}} - s_{i_{x_k}} \right| \tag{15}$$

The cost function related to the commutation of the MCSI and the buck converter is

$$c_{comm} = \lambda_{mcsi} N_{comm} + \lambda_{buck} \left| s_{b_{k+1}} - s_{b_k} \right| \tag{16}$$

where the weights λ_{buck} and λ_{mcsi} are chosen empirically to obtain the desired average switching frequency. To normalize all the terms of the global cost function, a weight factor is applied to each of them, given by

$$\lambda_{v_{ref}} = \frac{1}{e^2_{v_{ref}}} \qquad \lambda_{i_{dc}} = \frac{1}{e^2_{i_{dc}}} \tag{17}$$

where e_{vref} and $e_{i_{dc}}$ are the chosen error limits of the output voltage and buck current. Finally, the sum of the terms weighted by their factors leads to the global cost function,

$$\begin{aligned} c_{global} = \lambda_{v_{ref}} c_{v_{ref}} + \lambda_{i_{dc}} c_{i_{dc}} + \lambda_{csi} N_{comm} \\ + \lambda_{buck} \left| s_{b_{k+1}} - s_{b_k} \right| \end{aligned} \tag{18}$$

The switching state that minimize (18) is selected and applied at instant $k+1$.

TABLE II
SYSTEM PARAMETERS

Symbol	Definition	Value
V_{dc}	Voltage source	5kV
R_L	Load resistor	15Ω
L_L	Load inductor	$6mH$
L_{dc}	DC inductor	$120mH$
C_f	Filter capacitors	$22.2\mu F$
T_s	Sampling time	$200\mu s$
f_l	Reference frequency	50Hz
$i_{dc_{ref}}$	Reference current	200A
v_{ref}	Reference voltage	2.9kV
e_{vref}	Acceptable voltage error	$0.01\, v_{ref}$
$e_{i_{dc}}$	Acceptable current error	$0.01\, i_{dc_{ref}}$
λ_{mcsi}	Weighting factor for MCSI	$\frac{1}{3}$
λ_{buck}	Weighting factor for Buck	2

IV. SIMULATION RESULTS

The proposed control method is validated through simulations carried out using MATLAB/Simulink. The parameters used are shown in Table II. The prediction is done with a sampling time equal to T_s. In the following subsections the system behaviour is tested under nominal conditions, changes of the output voltage and a step of the input current reference.

A. Nominal conditions

The simulated waveforms of the inverter under nominal conditions are shown in Fig. 2. The output voltage tracks its references with minimal error as shown in Fig. 2a. This is achieved with a low switching frequency as depicted in Fig. 2d. Line to line voltage v_{ab} is presented in Fig. 2b. The output current i_a, presented in Fig. 2c, shows an almost

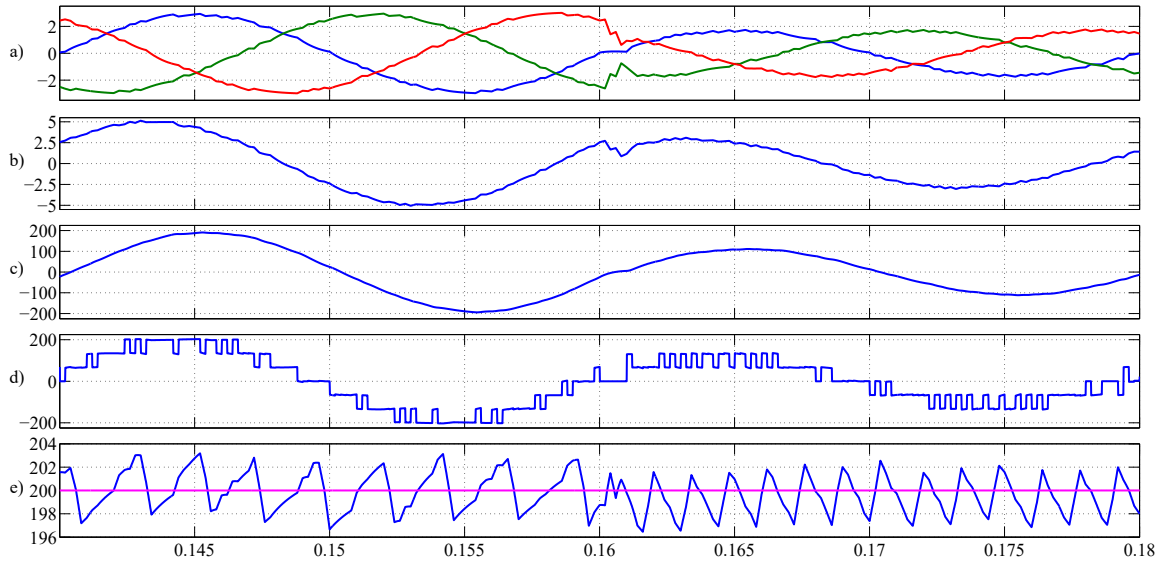

Fig. 4. Simulation results for predictive control of the system with a step change in voltage references; a) phase voltages and references [kV], b) line-to-line output voltage v_{ab} [kV], c) output current i_a [A], d) inverter output current of phase a [A], e) inductor current i_{dc} [A]

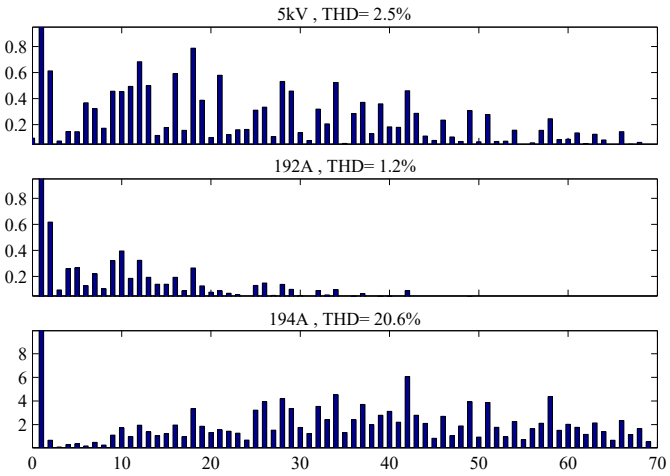

Fig. 3. Waveform spectrum versus harmonic order; a) line-to-line output voltage v_{ab} [V], b) output current i_a [A], c) inverter output i_{inv_a} [A]

sinusoidal waveform. In Fig. 2e, the output current of the buck converter is shown. It can be seen that it is tracking its reference with a low ripple of $\pm$ 3A. Under these conditions an average switching frequency of about 400Hz is obtained for the MCSI while the buck converter switch s_b presents an average switching frequency of 390Hz. Fig. 3 shows that the i_{inv_a} THD is approximately 20%, while the distortion of i_a is reduced to almost 1% due to the filter capacitors and the THD of line to line voltage, v_{ab}, is less than 2.5%.

B. Output Voltage Step

A step of the reference voltages from 2.9kV to 1.7kV is applied at time 0.16s. The results are shown in Fig. 4. The controller tracks almost immediately the reference change while the i_{dc} current remains around its own reference. In this case, the THD of v_{ab} and i_a increase to 4% and 1.9% respectively with an increment in the average switching frequency of the inverter up to 900Hz. The average switching frequency of the buck converter also increases to 650Hz. The ripple of i_{dc} remains practically constant as shown in Fig. 4e. The switching frequency increases because the switches of the MCSI jump to a zero state more frequently in order to achieve the lower output current caused by the change in the reference voltages. As expected, not every level of the output current are used due to the relation between the output and the input current of the inverter. The controller behaves robustly tracking the references under this conditions.

C. Current Input Step

While keeping the output voltage reference at 1.7kV, a negative step of 80A is applied to the current reference of the buck converter. These results can be seen on Fig. 5. The current i_{dc} settles in less than 12ms. After the current settles, the output voltage waveforms $v_{a,b,c}$ present a shape similar as in Sub. IV-A with 2.8% of voltage THD, 1.4% of current THD and an average switching frequency of the inverter equal to 550Hz. The main change observed is the average switching frequency of the buck converter that increases up to 700Hz in this case.

V. Conclusion

The predictive load voltage control strategy of a MCSI and its current source, which is implemented using a buck converter, has been presented. The discrete-time model of the plant has been described and used to predict the best suited switching state that must be applied at the next sampling period. The inclusion of the switching state of the buck converter within the controller allows the use of a non constant power source while controlling the current fed to the MCSI.

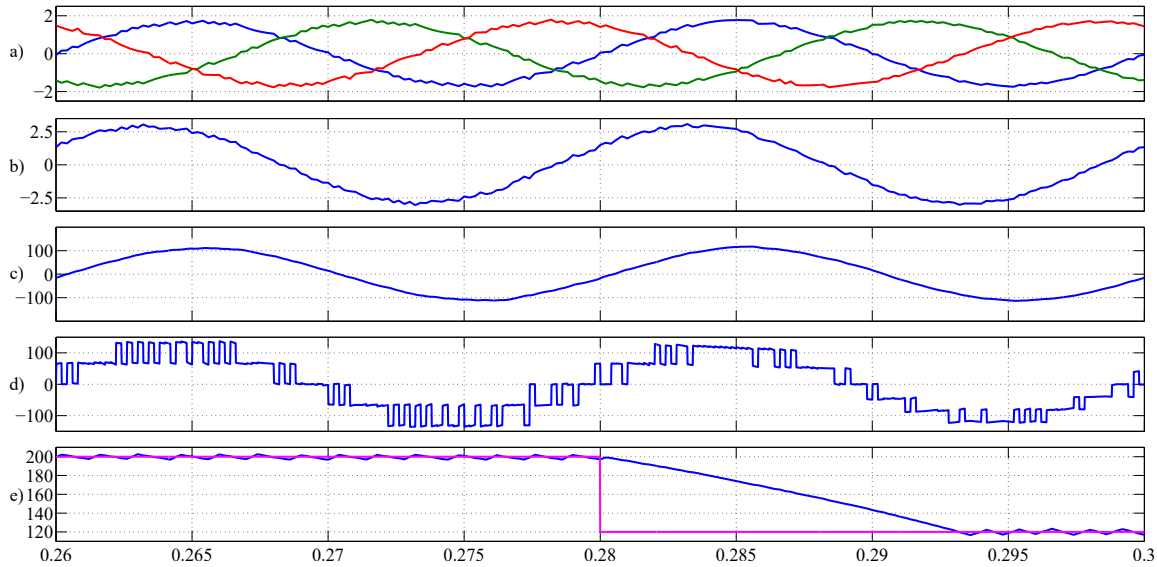

Fig. 5. Simulation results under a step change in current reference; a) phase voltages and references [kV], b) line-to-line output voltage v_{ab} [kV], c) output current i_a [A], d) inverter output current of phase a [A], e) inductor current i_{dc} [A]

Using a simple but effective cost function, the algorithm shows a good reference tracking and a significant reduction of the switching frequency of the inverter in comparison with the SPWM modulation under the same load and input conditions. In addition, this controller performs the balancing of the internal currents of the inverter and provides a low switching frequency of the buck converter, reducing switching losses and increasing the efficiency of the whole system. The proposed controller shows a robust behaviour under abrupt changes on both of its references while maintains the THD of the concerned waveforms below the limits imposed by the regulations.

REFERENCES

[1] R. Li, G. P. Adam, D. Holliday, J. E. Fletcher, and B. W. Williams, "Hybrid Cascaded Modular Multilevel Converter With DC Fault Ride-Through Capability for the HVDC Transmission System," *IEEE Transactions on Power Delivery*, vol. 30, no. 4, pp. 1853–1862, Aug 2015.

[2] E. S. Najmi and A. Ajami, "Modular symmetric and asymmetric reduced count switch multilevel current source inverter," *IET Power Electronics*, vol. 9, no. 1, pp. 51–61, 2016.

[3] P. Cossutta, M. P. Aguirre, A. Cao, S. Raffo, and M. I. Valla, "Single-Stage Fuel Cell to Grid Interface With Multilevel Current-Source Inverters," *IEEE Transactions on Industrial Electronics*, vol. 62, no. 8, pp. 5256–5264, Aug 2015.

[4] N. Mittal, B. Singh, S. Singh, R. Dixit, and D. Kumar, "Multilevel Inverters: A Literature Survey on Topologies and Control Strategies," in *Power, Control and Embedded Systems (ICPCES), 2012 2nd International Conference on*, Dec 2012, pp. 1–11.

[5] S. Jayalath and M. Hanif, "Controller Tuning for a Single Phase Grid-Connected Current Source Inverter," in *Future Energy Electronics Conference (IFEEC), 2015 IEEE 2nd International*, Nov 2015, pp. 1–6.

[6] S. Anand, S. K. Gundlapalli, and B. G. Fernandes, "Transformer-Less Grid Feeding Current Source Inverter for Solar Photovoltaic System," *IEEE Transactions on Industrial Electronics*, vol. 61, no. 10, pp. 5334–5344, Oct 2014.

[7] R. Errouissi, A. Al-Durra, and S. M. Muyeen, "Design and Implementation of a Nonlinear PI Predictive Controller for a Grid-Tied Photovoltaic Inverter," *IEEE Transactions on Industrial Electronics*, vol. PP, no. 99, pp. 1–1, 2016.

[8] S. Kouro, M. A. Perez, J. Rodriguez, A. M. Llor, and H. A. Young, "Model Predictive Control: MPC's Role in the Evolution of Power Electronics," *IEEE Industrial Electronics Magazine*, vol. 9, no. 4, pp. 8–21, Dec 2015.

[9] L. Ben-Brahim, A. Gastli, M. Trabelsi, K. Ghazi, M. Houchati, and H. Abu-Rub, "Modular Multilevel Converter Circulating Current Reduction Using Model Predictive Control," *IEEE Transactions on Industrial Electronics*, vol. PP, no. 99, pp. 1–1, 2016.

[10] Z. Shu, M. Liu, L. Zhao, S. Song, Q. Zhou, and X. He, "Predictive Harmonic Control and Its Optimal Digital Implementation for MMC-Based Active Power Filter," *IEEE Transactions on Industrial Electronics*, vol. 63, no. 8, pp. 5244–5254, Aug 2016.

[11] D. K. Choi and K. B. Lee, "Dynamic Performance Improvement of AC/DC Converter Using Model Predictive Direct Power Control With Finite Control Set," *IEEE Transactions on Industrial Electronics*, vol. 62, no. 2, pp. 757–767, Feb 2015.

[12] O. Abdel-Rahim and H. Funato, "Five-Level Multilevel Power Conditioning System for Grid-Tie Photovoltaic Applications with Novel Model Predictive Control," in *Future Energy Electronics Conference (IFEEC), 2015 IEEE 2nd International*, Nov 2015, pp. 1–6.

[13] J. Rodriguez, S. Bernet, P. K. Steimer, and I. E. Lizama, "A Survey on Neutral-Point-Clamped Inverters," *IEEE Transactions on Industrial Electronics*, vol. 57, no. 7, pp. 2219–2230, July 2010.

[14] C. Du, J. Zhou, and Y. Ma, "Predictive Current Control of a Current-Source Inverter with Active Damping Method," in *Energy Conversion Congress and Exposition (ECCE), 2015 IEEE*, Sept 2015, pp. 1100–1104.

[15] K. R. Sree and A. K. Rathore, "Impulse Commutated High-frequency Soft-switching Modular Current-fed Three-phase DC/DC Converter for Fuel Cell Applications," *IEEE Transactions on Industrial Electronics*, vol. PP, no. 99, pp. 1–1, 2016.

[16] Q. Wu, Q. Wang, J. Xu, H. Li, and L. Xiao, "A High Efficiency Step-Up Current-Fed Push-Pull Quasi-Resonant Converter with Fewer Components for Fuel Cell Application," *IEEE Transactions on Industrial Electronics*, vol. PP, no. 99, pp. 1–1, 2016.

[17] A. Chub, D. Vinnikov, R. Kosenko, and L. Liivik, "Wide Input Voltage Range Photovoltaic Microconverter with Reconfigurable Buck-Boost Switching Stage," *IEEE Transactions on Industrial Electronics*, vol. PP, no. 99, pp. 1–1, 2016.

[18] M. Z. JamalAbadi, M. Mohamadian, and R. Beiranvand, "A Single-Phase Grid-Connected Photovoltaic Inverter Based on a Three-Switch Three-Port Flyback with Series Power Decoupling Circuit," *IEEE Transactions on Industrial Electronics*, vol. PP, no. 99, pp. 1–1, 2016.